CHAPTER IV

NUMERICAL RESULTS AND DISCUSSION

In this chapter, results from an extensive parametric study to investigate the influence of the thickness on the distribution of the stress intensity factor along the crack front of the CT specimen are reported and discussed. In the analysis, the specimen thickness is varied from $t/a = 1$ to $t/a = 40$ to ensure that the plane strain condition dominates the majority of the crack front of the specimen with the maximum thickness $t/a = 40$. Two important classes of linear elastic materials, one associated with isotropic materials and the other corresponding to transversely isotropic materials, are examined in the present study. Meshes generated using the strategy described in section 3.4 and section 3.7 are utilized in the analysis for the stress intensity factor.

4.1 Results for isotropic materials

To explore the influence of the specimen thickness and material constants on the behavior of the stress intensity along the crack front for the isotropic case, we perform the analysis for various thicknesses $t/a \in \{1, 2, 3, 4, 5, 10, 20, 40\}$ and several values of Poisson's ratio $\nu \in \{0,\ 0.05,\ 0.10,\ 0.15,\ 0.20,\ 0.25,\ 0.30,\ 0.35,\ 0.40,\ 0.45,\ 0.50\}$ for each thickness. It should be noted that the stress intensity factor exhibits material dependence only on the Poisson's ratio ν not the Young's modulus E. The normalized mode-I stress intensity factors, denoted by $K_I t\sqrt{W}/P$ where P is the total applied load and t and W are the specimen thickness and width, respectively, as indicated in Figure 3.2, is reported as a function of the normalized distance along the crack front, denoted by s/t where s is the distance measured from the center of the crack front, in Figure 4.1 for $\nu = 0$, Figure 4.2 for $\nu = 0.10$, Figure 4.3 for $\nu = 0.30$, and Figure 4.4 for $\nu = 0.50$ (results for other values of Poisson's ratio are shown in Appendix A). For each plot, the plane strain stress intensity factor proposed by ASTM E-399 is also reported to allow the comparison and discussion. From this set of results, following findings are summarized.

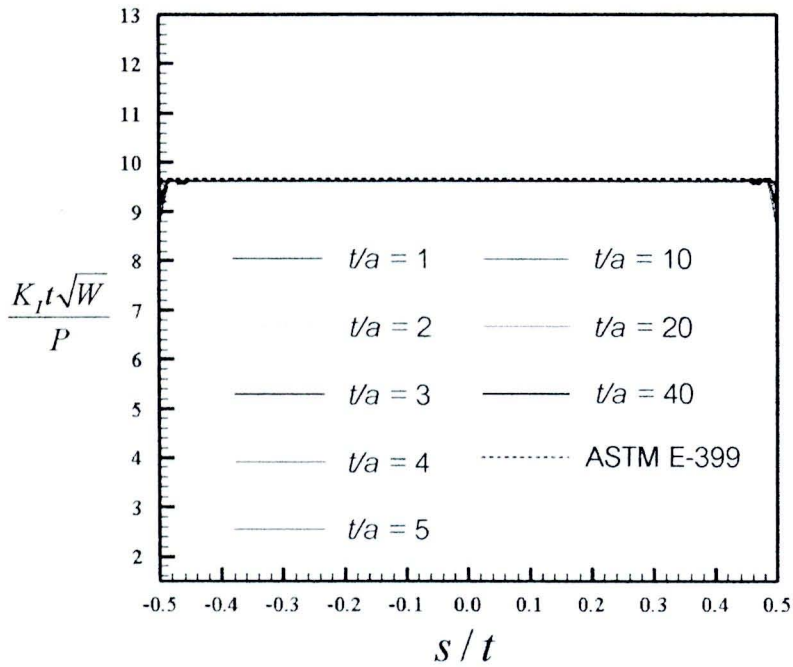

Figure 4.1 Normalized mode-I stress intensity factor versus the normalized distance along the crack front for various thicknesses and ν = 0

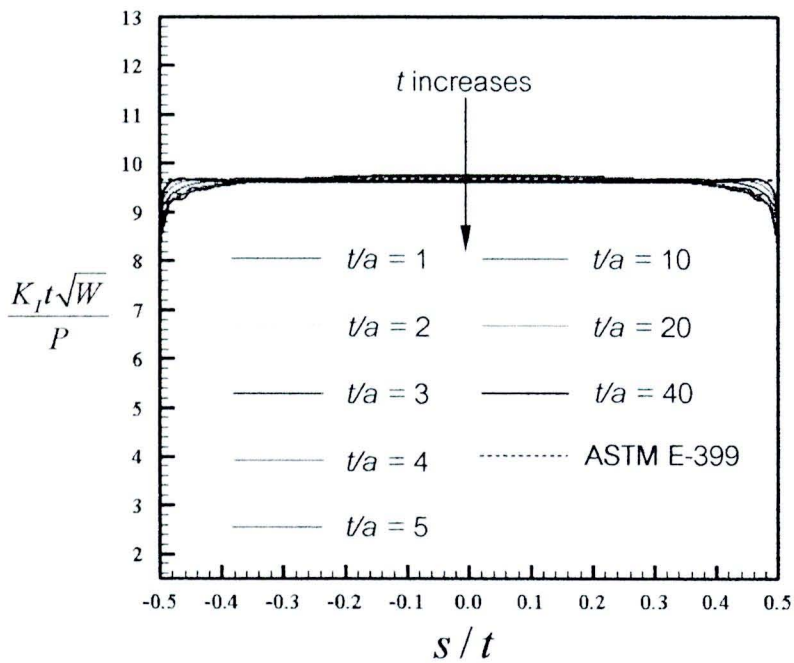

Figure 4.2 Normalized mode-I stress intensity factor versus the normalized distance along the crack front for various thicknesses and ν = 0.1

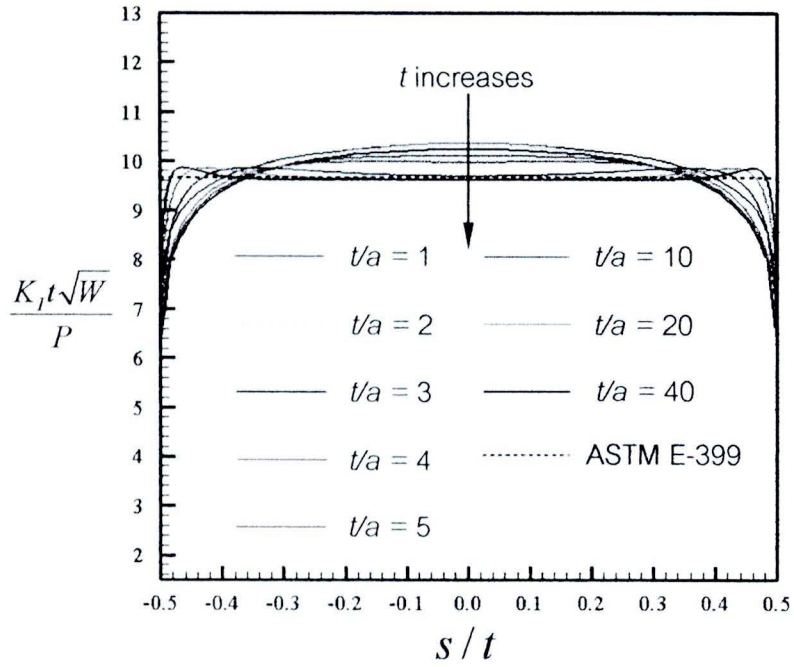

Figure 4.3 Normalized mode-I stress intensity factor versus the normalized distance along the crack front for various thicknesses and ν = 0.3

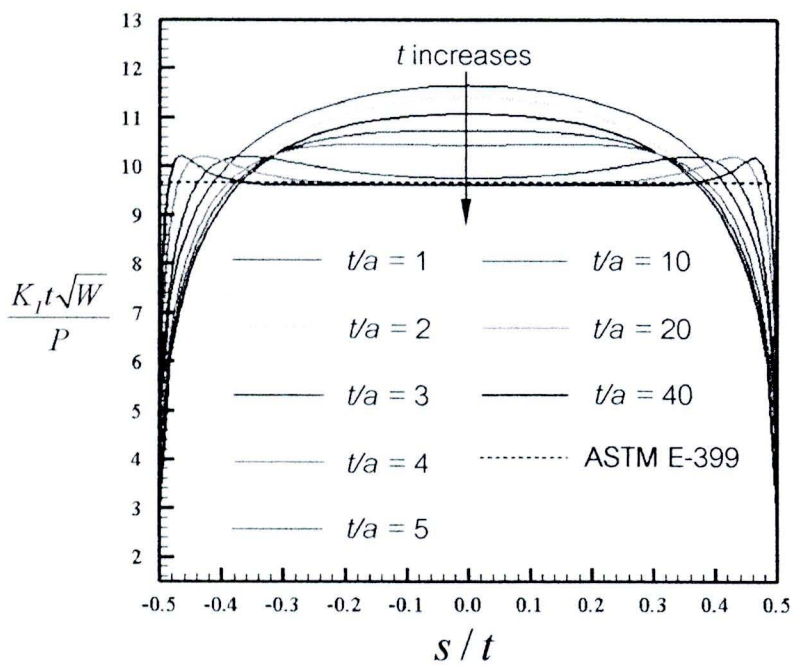

Figure 4.4 Normalized mode-I stress intensity factor versus the normalized distance along the crack front for various thicknesses and ν = 0.5

- For Poisson's ratio $\nu = 0$, the plane strain condition dominates the entire crack front with no regard of the specimen thickness and, in addition, the computed results exhibit excellent agreement with the benchmark solution except in the region close to the surface breaking points. The slightly oscillated behavior of numerical solutions observed in that region is due to the fact that the (reduced-order) special crack-tip element and the adjacent modified boundary element containing the vertices cannot accurately capture the asymptotic field. Note in addition that the stress field at the vertex, for this particular case, is singular of the same order as that for the interior point of the crack front.
- For small Poisson's ratio (i.e. $\nu \leq 0.1$), the stress intensity factor varies along the crack front but such variation is still insignificant for all thicknesses considered. The rapid decrease of the stress intensity factor is observed in the neighborhood of the surface breaking point. This implies that the singularity of the stress field at the vertex is of order less than $1/\sqrt{r}$.
- For moderate and large Poisson's ratio (i.e. $\nu \geq 0.2$), the variation of the stress intensity factor across the thick becomes more significant and depends primarily on the specimen thickness. For a specimen with small thickness (i.e. $t/a \leq 5$), the stress intensity factor attains its maximum value at the center of the crack front and monotonically decreases to zero at the two vertices. The slight rate of decrease is observed for the majority of the crack front except in a layer near the outer boundary where the rapid drop occurs. In addition, the three-dimensional analysis yields the stress intensity factor higher than the plane strain value for a large portion of the crack front. For a specimen with sufficiently large thickness (i.e. $t/a \geq 10$), the stress intensity factor starts to converge to the plane strain value in the central region

of the crack front and the converged zone spreads towards the vertices as the thickness increases.

- For a specimen with the maximum thickness $t/a = 40$, the plane strain dominated zone covers more than 70% of the crack front for all values of Poisson's ratio treated.

To additionally demonstrate the influence of the Poisson's ratio on both the distribution and magnitude of the stress intensity factor across the thickness, we create different plots between $K_I t\sqrt{W}/P$ and s/t by fixing the specimen thickness but varying the Poisson's ratio. Results are reported in Figure 4.5 for a thinnest specimen ($t/a = 1$), in Figure 4.6 for $t/a = 5$, in Figure 4.7 for $t/a = 10$, and in Figure 4.8 for $t/a = 40$. It can be concluded from these plots that the thickness of a specimen significantly affects the characteristic of the distribution (i.e. shape) of the stress intensity factor along the crack front while the Poisson's ratio only influence its magnitude. More specifically, the larger the Poisson's ratio, the higher the stress intensity factor is observed.

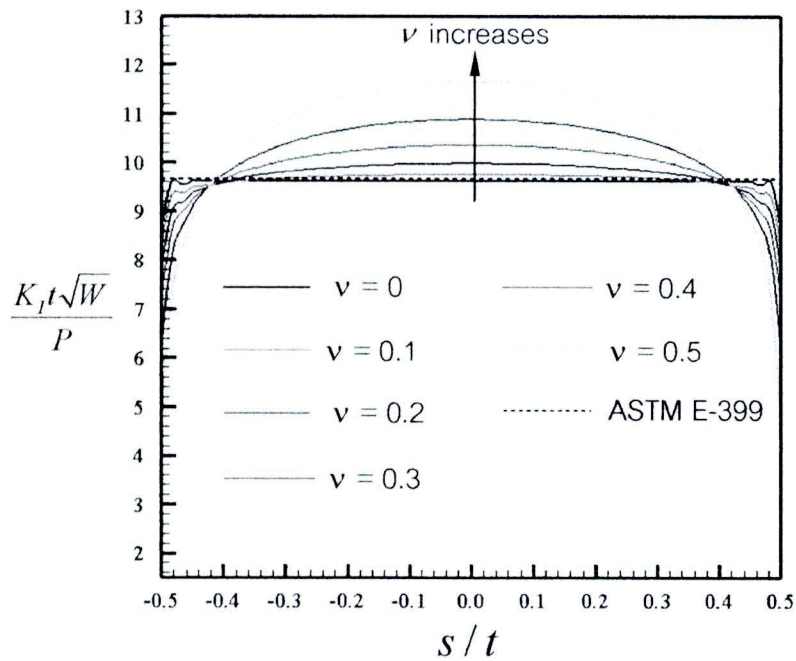

Figure 4.5 Normalized mode-I stress intensity factor versus the normalized distance along the crack front for various Poisson's ratios and $t/a = 1$

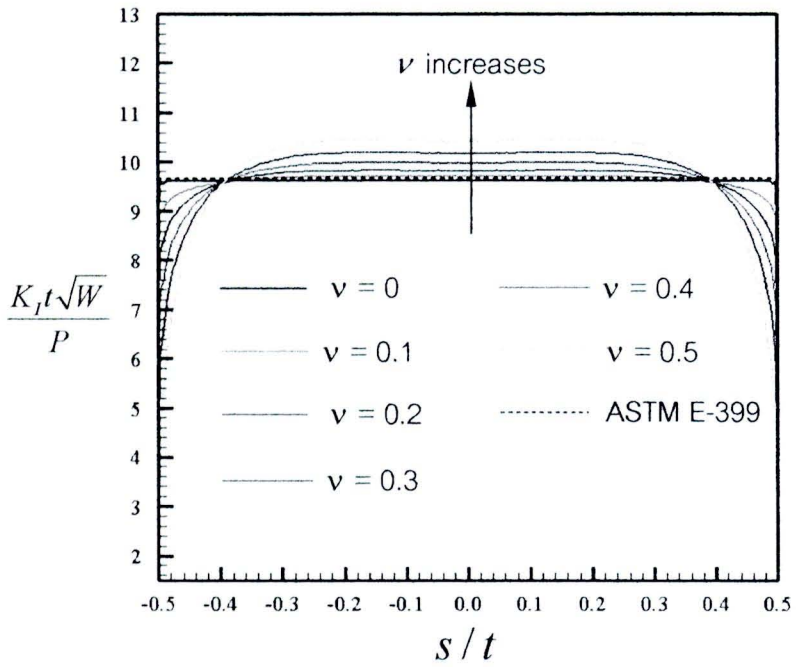

Figure 4.6 Normalized mode-I stress intensity factor versus the normalized distance along the crack front for various Poisson's ratios and $t/a = 5$

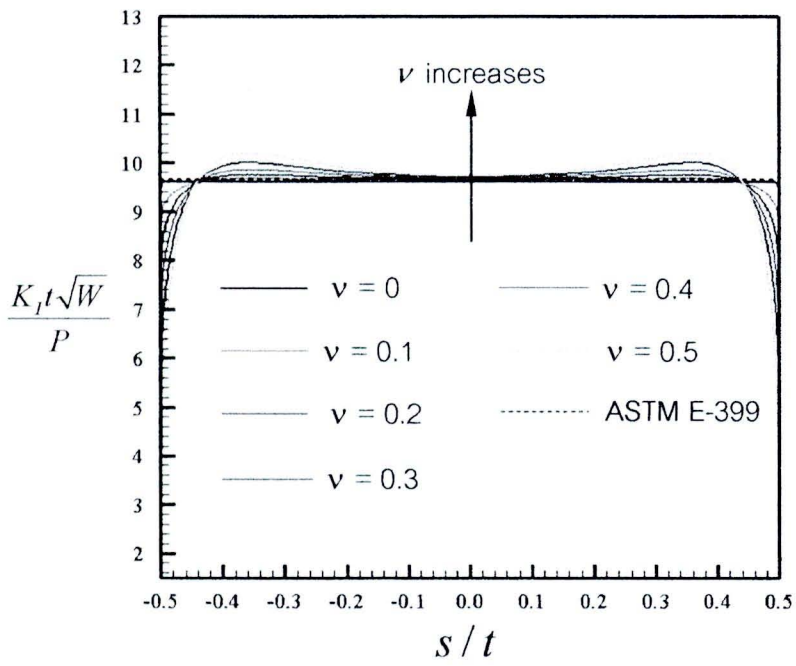

Figure 4.7 Normalized mode-I stress intensity factor versus the normalized distance along the crack front for various Poisson's ratios and $t/a = 10$

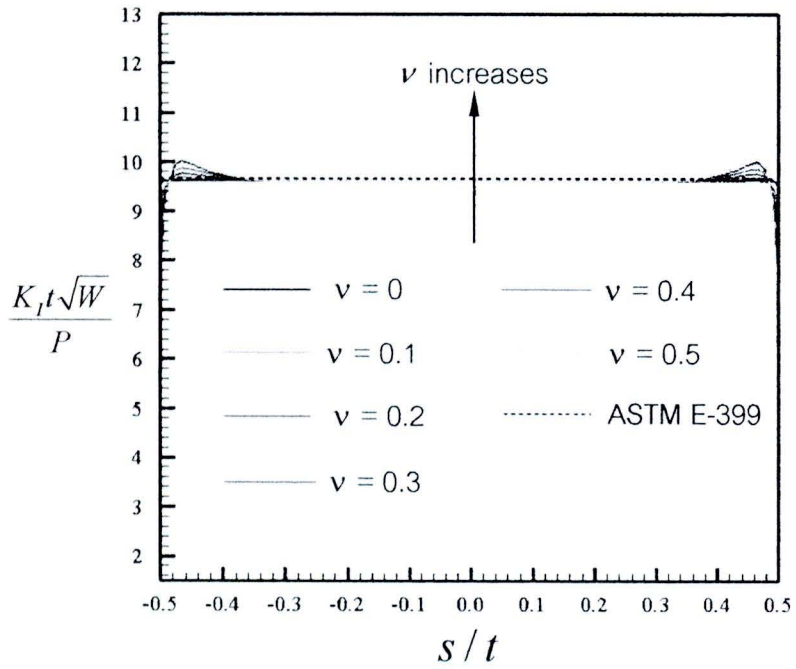

Figure 4.8 Normalized mode-I stress intensity factor versus the normalized distance along the crack front for various Poisson's ratios and $t/a = 40$

Next, we calculate the average of the stress intensity factor over the entire crack front from

$$\overline{K}_I = \int_{-t/2}^{t/2} K_I(s)ds \tag{4.1}$$

where $\overline{K}_I$ denotes the average of the stress intensity factor across the thickness and K_I is the computed stress intensity along the crack front. Although K_I is obtained only at nodes along the crack front, values at all other points can readily be obtained using quadratic interpolation functions (this choice of interpolation functions is not arbitrary but chosen to be consistent with the special crack-tip elements used in the weakly singular SGBEM) as follows:

$$K_I(s) = \frac{(s-s_2)(s-s_3)}{(s_1-s_2)(s_1-s_3)}K_I(s_1) + \frac{(s-s_1)(s-s_3)}{(s_2-s_1)(s_2-s_3)}K_I(s_2) + \frac{(s-s_1)(s-s_2)}{(s_3-s_1)(s_3-s_2)}K_I(s_3) \tag{4.2}$$

where $K_I(s_1)$, $K_I(s_2)$ and $K_I(s_3)$ are stress intensity factors at nodes along the crack front of the same crack tip element and s_1, s_2, s_3 are distances from the center of the crack front to those three nodes. To demonstrate the influence of the specimen thickness on the existence of the plane strain dominated zone and its size, we plot the average stress intensity factor $\bar{K}_I$, normalized by the plane strain solution K_{PS} (obtained by taking the converged stress intensity factor at the center of the crack front of a specimen with the thickness $t/a = 40$), versus the normalized specimen thickness t/a as shown in Figure 4.9. It is evident that for all Poisson's ratios greater than zero, $\bar{K}_I$ monotonically decreases and asymptotically converges to K_{PS} as the specimen thickness increases. This finding along with results shown in Figures 4.1-4.4 implies that once the plane strain dominated zone exists along the crack front, its size becomes larger as the specimen thickness increases. Furthermore, the rate of convergence to the plane strain solution decreases as the Poisson's ratio increases. This clearly indicates that a specimen made of a material with higher Poisson's ratio requires larger thickness to achieve the same level of plane strain condition along the crack front.

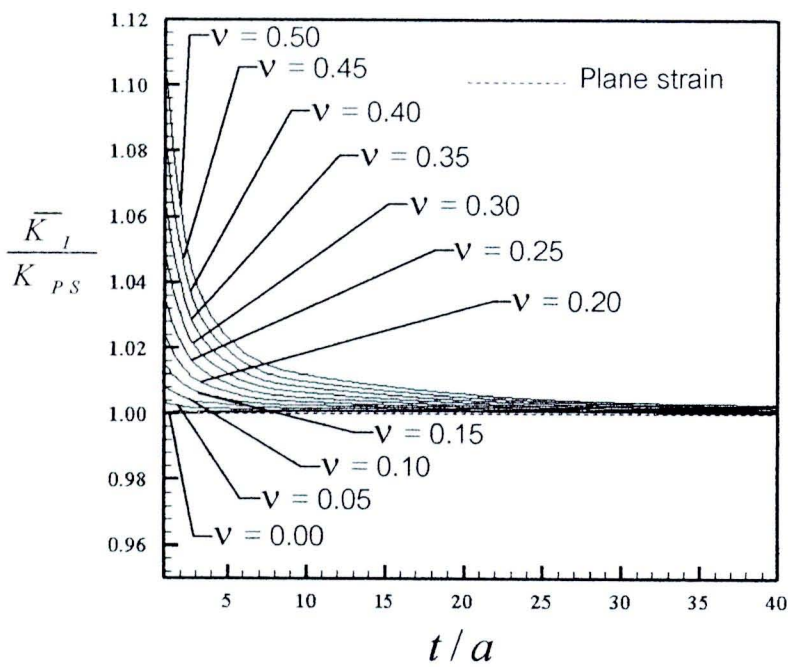

Figure 4.9 Normalized average stress intensity factor versus normalized thickness for various Poisson's ratios

In addition, an empirical relation between the normalized average stress intensity factor $\bar{K}_I / K_{ps}$ and the normalized specimen thickness t/a for any Poisson's ratio can readily be obtained from a standard curve-fitting technique. Based on the data shown in Figure 4.9, a hyperbola function form is suggested in the curve fitting procedure and the final empirical formula is given by

$$\frac{\bar{K}_I}{K_{PS}} = 1 + \frac{0.4008\nu^2 + 0.0591\nu - 0.001}{\frac{t}{a} + 197.05\nu^4 - 298.69\nu^3 + 167.57\nu^2 - 42.76\nu + 4.7006} \tag{4.3}$$

where ν is the Poisson's ratio. Figure 4.10 shows plots between $\bar{K}_I / K_{ps}$ and t/a obtained from the formula (4.3) and from the analysis by the SGBEM. It is evident that the formula (4.3) shows excellent agreement with numerical results for a wide range of the Poisson's ratio and, as a result, can be used confidently to predict the average stress intensity factor for a given specimen thickness and Poisson's ratio.

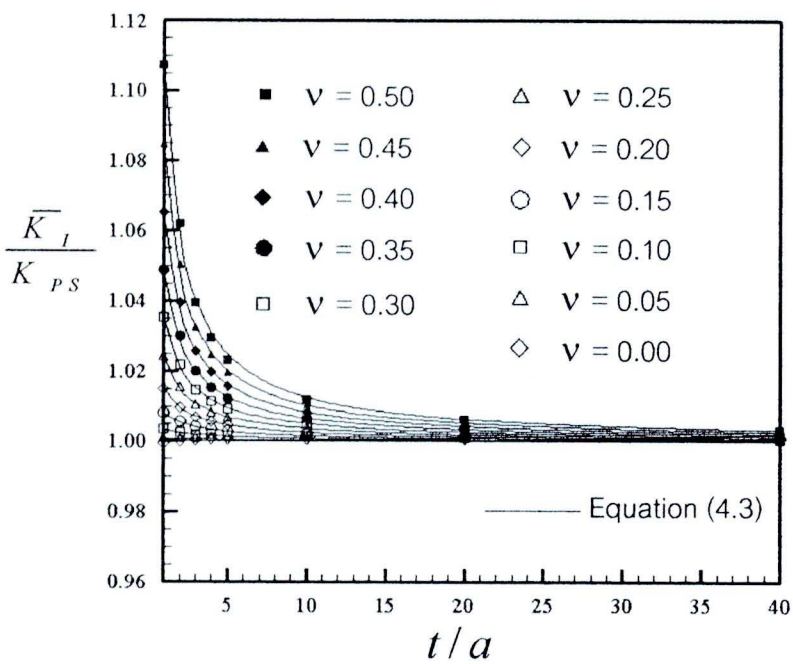

Figure 4.10 Normalized average stress intensity factor versus normalized thickness obtained from equation (4.3) and from analysis data

4.2 Results for transversely isotropic materials

A brief description of a constitutive equation and independent material constants for transversely isotropic materials is given here first to clearly identify some parameters chosen in the parametric study. The six stress components $\{\sigma_{11}, \sigma_{22}, \sigma_{33}, \sigma_{12}, \sigma_{23}, \sigma_{13}\}$ and the six strain components $\{\varepsilon_{11}, \varepsilon_{22}, \varepsilon_{33}, \varepsilon_{12}, \varepsilon_{23}, \varepsilon_{13}\}$ for this particular class of materials (with the axis of material symmetry directing along the X_3-axis and perpendicular to the crack plane) are related by five independent material constants via following two equivalent constitutive equations (e.g. Staab, 1999 and Singh, 2007)

$$\begin{Bmatrix} \sigma_{11} \\ \sigma_{22} \\ \sigma_{33} \\ \sigma_{12} \\ \sigma_{23} \\ \sigma_{13} \end{Bmatrix} = \begin{bmatrix} E_{1111} & E_{1122} & E_{1133} & 0 & 0 & 0 \\ E_{1122} & E_{1111} & E_{1133} & 0 & 0 & 0 \\ E_{1133} & E_{1133} & E_{3333} & 0 & 0 & 0 \\ 0 & 0 & 0 & (E_{1111}-E_{1122}) & 0 & 0 \\ 0 & 0 & 0 & 0 & E_{1313} & 0 \\ 0 & 0 & 0 & 0 & 0 & E_{1313} \end{bmatrix} \begin{Bmatrix} \varepsilon_{11} \\ \varepsilon_{22} \\ \varepsilon_{33} \\ 2\varepsilon_{12} \\ 2\varepsilon_{23} \\ 2\varepsilon_{13} \end{Bmatrix} \tag{4.4}$$

$$\begin{Bmatrix} \varepsilon_{11} \\ \varepsilon_{22} \\ \varepsilon_{33} \\ 2\varepsilon_{12} \\ 2\varepsilon_{23} \\ 2\varepsilon_{13} \end{Bmatrix} = \begin{bmatrix} 1/E_p & -\nu_p/E_p & -\nu_{zp}/E_z & 0 & 0 & 0 \\ -\nu_p/E_p & 1/E_p & -\nu_{zp}/E_z & 0 & 0 & 0 \\ -\nu_{pz}/E_p & -\nu_{pz}/E_p & 1/E_z & 0 & 0 & 0 \\ 0 & 0 & 0 & 2(1+\nu_p)/E_p & 0 & 0 \\ 0 & 0 & 0 & 0 & 1/G_{zp} & 0 \\ 0 & 0 & 0 & 0 & 0 & 1/G_{zp} \end{bmatrix} \begin{Bmatrix} \sigma_{11} \\ \sigma_{22} \\ \sigma_{33} \\ \sigma_{12} \\ \sigma_{23} \\ \sigma_{13} \end{Bmatrix} \tag{4.5}$$

where $E_{1111}, E_{1122}, E_{1133}, E_{3333}$ and E_{1313} are five independent elastic constants; E_p and ν_p are the Young's modulus and Poisson's ratio in the $X_1 - X_2$ symmetry plane; E_z, G_{zp} and ν_{pz} (or ν_{zp}) are the Young's modulus, shear modulus and Poisson's ratio in the X_3 direction; and the two Poisson's ratios are not independent but related through $\nu_{pz}/E_p = \nu_{zp}/E_z$.

In the parametric study, we first investigate the influence of the specimen thickness on behavior of the stress intensity factor along the crack front for two particular transversely isotropic materials (i.e. zinc and cadmium) and then the influence of the

Poisson's ratio ν_p, the modulus ratio E_p / E_z and the modulus ratio G_{zp} / E_p are thoroughly examined.

4.2.1 Results for zinc and cadmium

For this particular case, we perform numerical experiments for various thicknesses $t/a \in \{1,2,3,4,5,10,20,40\}$ by using the same meshes as those employed in the isotropic case. The elastic constants for zinc and cadmium used in the analysis are given in Table 3.2. The normalized mode-I stress intensity factor ($K_I t\sqrt{W}/P$) are reported as a function of the normalized distance along the crack front (s/t) in Figure 4.11 for zinc and in Figure 4.12 for cadmium. The average stress intensity factor (computed based on equations (4.1) and (4.2)) normalized by the plane strain solution (obtained by taking the converged stress intensity factor at the center of the crack front of a specimen with the thickness $t/a = 40$) is shown in Figure 4.13 as a function of the normalized thickness. From this set of results, it can be concluded that

- The computed stress intensity factors for zinc and cadmium exhibit only slight difference, both in terms of the distribution and magnitude, for all thicknesses considered in the analysis. In addition, the average stress intensity factor for zinc is slightly higher than that for cadmium.
- For thin specimens ($t/a \leq 5$), the distribution of the stress intensity factor possesses the same characteristic as that for the isotropic case. For instance, the maximum stress intensity factor still occurs at the center of the crack front and drop rapidly at the region close to the vertices. In addition, the stress intensity factor is higher than the plane strain solution for the majority of the crack front and no plane strain dominated zone is observed in this range of thickness.
- For sufficiently thick specimen ($t/a \geq 10$), the plane strain dominated zone is observed in the central region of the crack front. Similar to the isotropic case, as the specimen thickness increases, this zone expands towards the outer boundary.
- As clearly demonstrated by Figure 4.13, the average stress intensity factor decreases monotonically and asymptotically converges to the plane strain solution as the specimen thickness increases. In

particular, for a specimen with the thickness $t/a \geq 5$, the difference between $\bar{K}_I$ and K_{PS} is less than 2% whereas a specimen with the thickness $t/a \geq 10$, the difference reduce to a fraction of 1%.

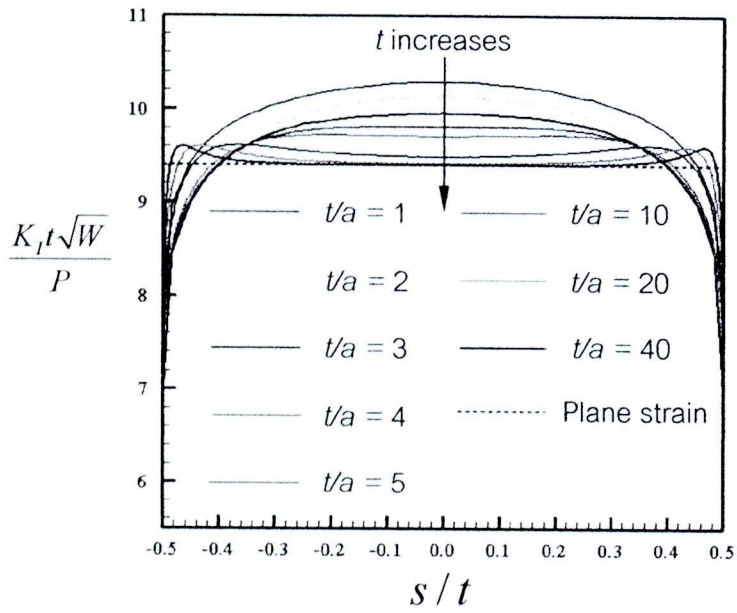

Figure 4.11 Normalized mode-I stress intensity factor versus the normalized distance along the crack front for zinc

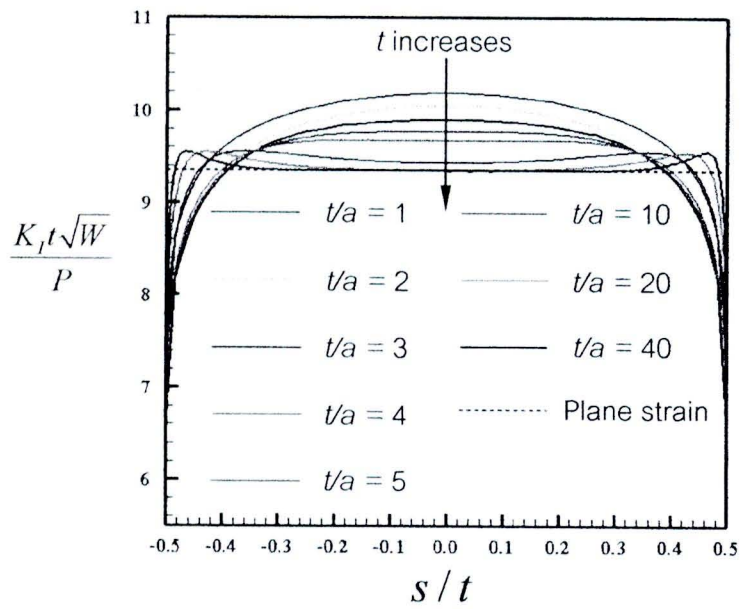

Figure 4.12 Normalized mode-I stress intensity factor versus the normalized distance along the crack front for cadmium

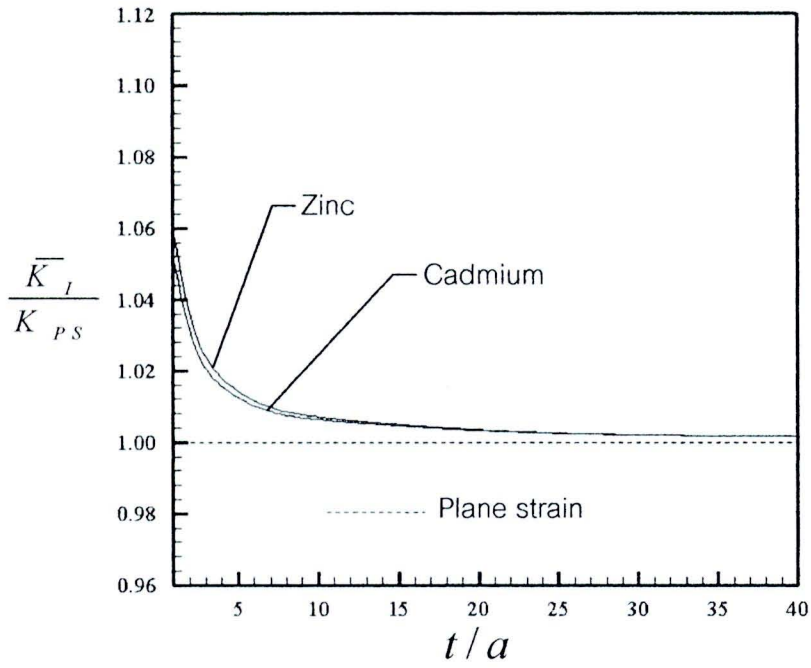

Figure 4.13 Normalized average stress intensity factor versus normalized thickness for zinc and cadmium

4.2.2 Influence of Poisson's ratio ν_p

Next, we investigate the influence of Poisson's ratio ν_p in the $X_1 - X_2$ symmetry plane on the distribution of the stress intensity factor for various thicknesses. In numerical experiments, all other four material constants are fixed except the Poisson's ratio ν_p that is varied over its entire range. The fixed material constants (i.e. E_p, E_z, G_{zp} and ν_{pz} (and ν_{zp})) are taken from those for cadmium as given in Table 4.1. Seven values of Poisson's ratio, i.e. $\nu_p \in \{0.00, 0.10, 0.20, 0.30, 0.40, 0.50, 0.60\}$, are considered and the corresponding elastic constants employed in the SGBEM are shown in Table 4.2.

Table 4.1 Material constants for cadmium used in the investigation of ν_p

Material	E_p (GPa)	E_z (GPa)	G_{zp} (Gpa)	ν_p	ν_{pz}	ν_{zp}
Cadmium	83.0	30.0	20.0	0.10	0.70	0.26

Table 4.2 Elastic constants (GPa) associated with different values of Poisson's ratio (ν_p). The axis of material symmetry is taken to direct along the x_3-coordinate direction.

Materials	E_{1111}	E_{1122}	E_{1133}	E_{3333}	E_{1313}
ν_p=0.00	106.8	23.8	33.9	47.2	20.0
ν_p=0.10	115.2	39.7	40.3	50.4	20.0
ν_p=0.20	129.8	60.6	49.5	55.0	20.0
ν_p=0.30	155.4	91.6	64.2	62.5	20.0
ν_p=0.40	205.5	146.2	91.4	76.3	20.0
ν_p=0.50	332.8	277.5	158.7	110.3	20.0
ν_p=0.60	1178.7	1126.8	599.4	333.3	20.0

Results obtained from this extensive analysis reveal that the distribution of the stress intensity factor along the crack front for both thin and thick specimens possesses the same characteristic as that for zinc and cadmium as clearly demonstrated in Figures 4.14-4.16 for $\nu_p = 0, 0.3, 0.6$ (results for other values of are shown in Appendix B). The Poisson's ratio ν_p only influences the magnitude of the stress intensity factor for a given specimen thickness as indicated in Figures 4.17-4.20 for $t/a = 1, 5, 10, 40$. It is important to point out that results for $\nu_p = 0$ possess totally different behavior from those for the isotropic case with $\nu = 0$. No independence of the specimen thickness is observed for the case of transversely isotropic materials.

The average stress intensity factor $\bar{K}_I$ for different values of ν_p is also reported as a function of the normalized thickness in Figure 4.21. Similar to the isotropic case, obtained results confirmed that as the Poisson's ratio ν_p increases, $\bar{K}_I$ monotonically converges to the plane strain solution with a slower rate. Note in particular that the difference between $\bar{K}_I$ and K_{PS} is less than 2% for a specimen with the thickness $t/a \geq 5$ and less than 1% for a specimen with the thickness $t/a \geq 10$.

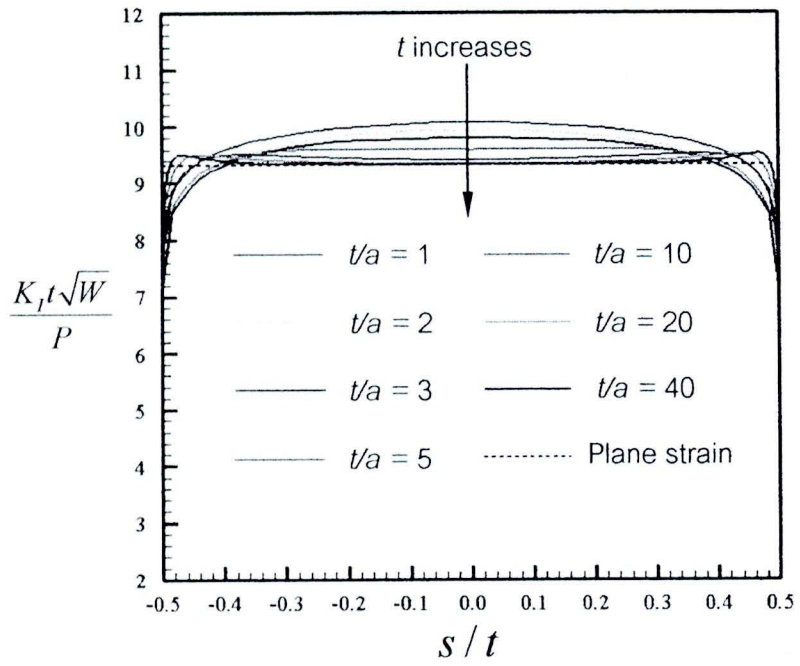

Figure 4.14 Normalized mode-I stress intensity factor versus the normalized distance along the crack front for various thicknesses and ν_p = 0

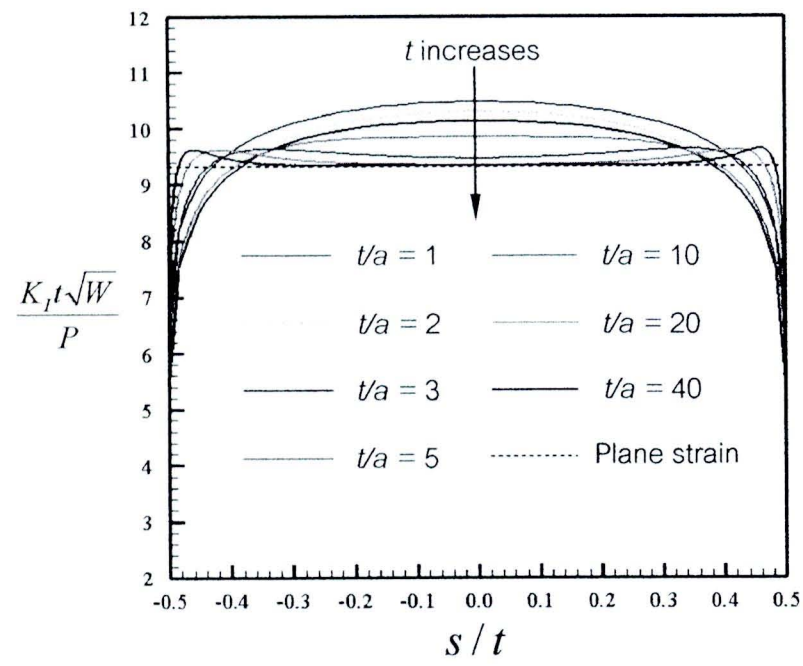

Figure 4.15 Normalized mode-I stress intensity factor versus the normalized distance along the crack front for various thicknesses and ν_p = 0.3

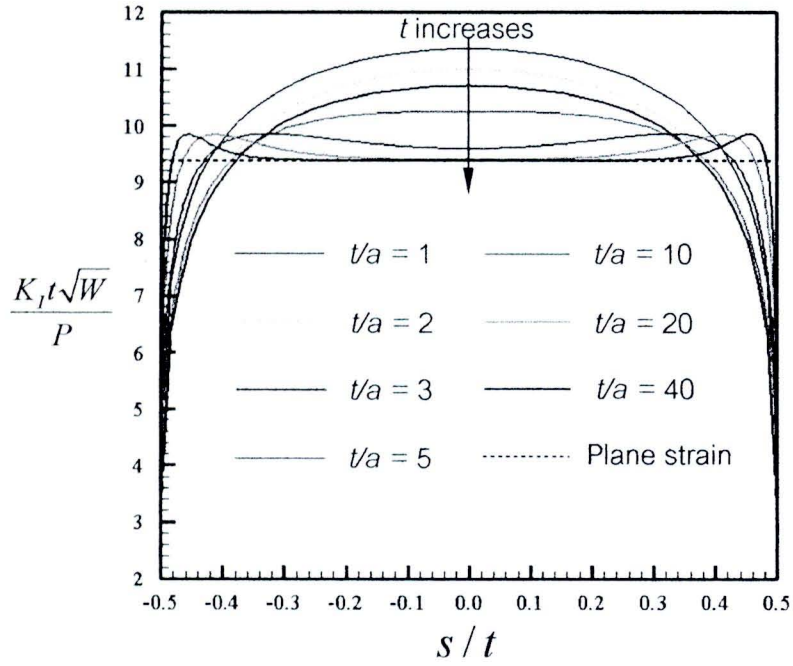

Figure 4.16 Normalized mode-I stress intensity factor versus the normalized distance along the crack front for various thicknesses and ν_p = 0.6

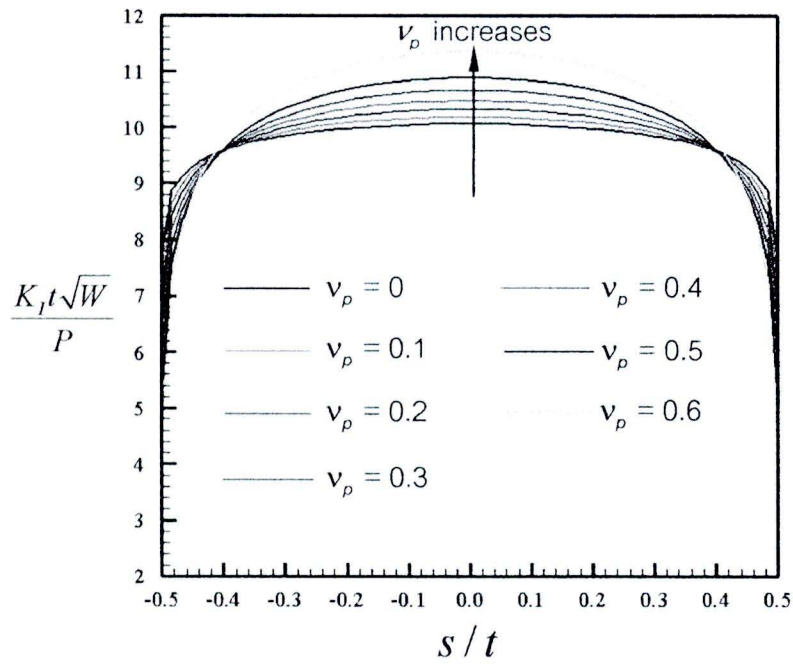

Figure 4.17 Normalized mode-I stress intensity factor versus the normalized distance along the crack front for various Poisson's ratios and $t/a = 1$

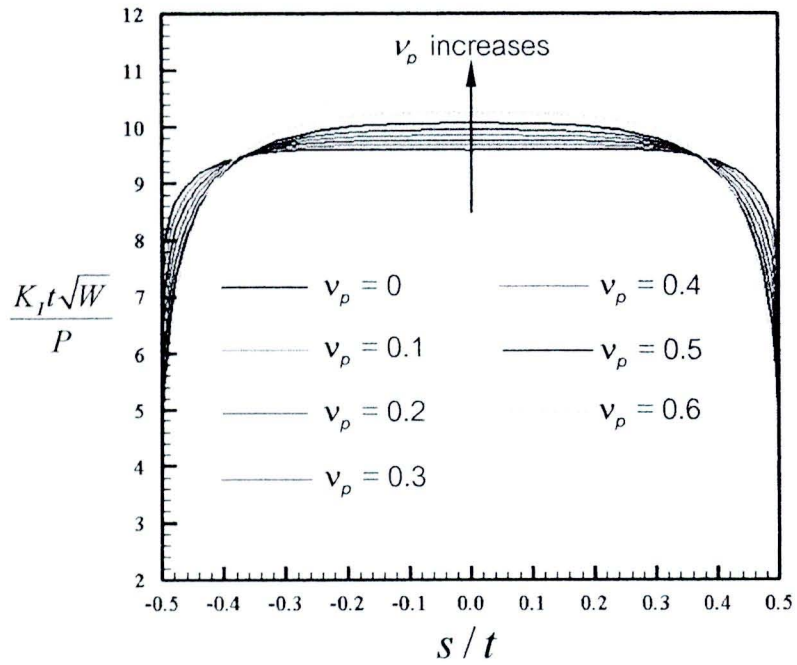

Figure 4.18 Normalized mode-I stress intensity factor versus the normalized distance along the crack front for various Poisson's ratios and $t/a = 5$

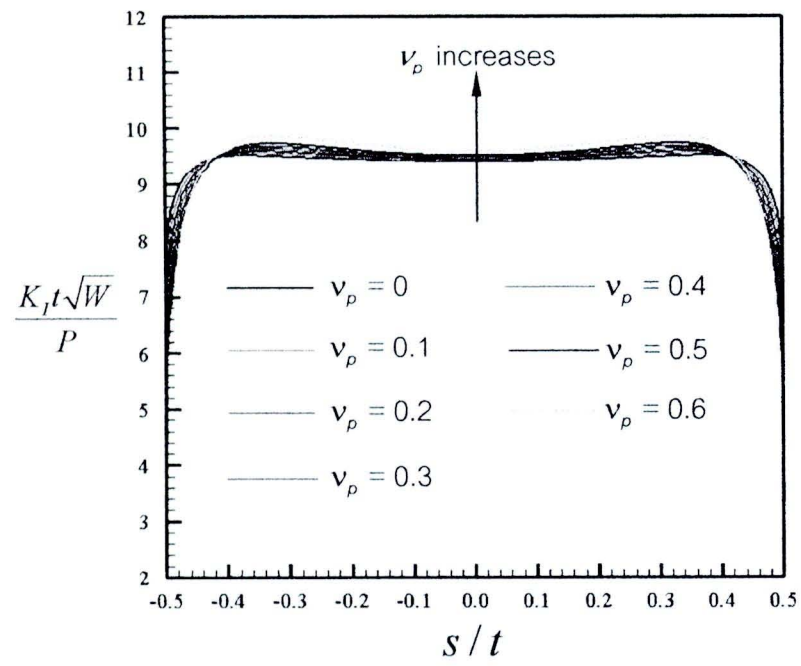

Figure 4.19 Normalized mode-I stress intensity factor versus the normalized distance along the crack front for various Poisson's ratios and $t/a = 10$

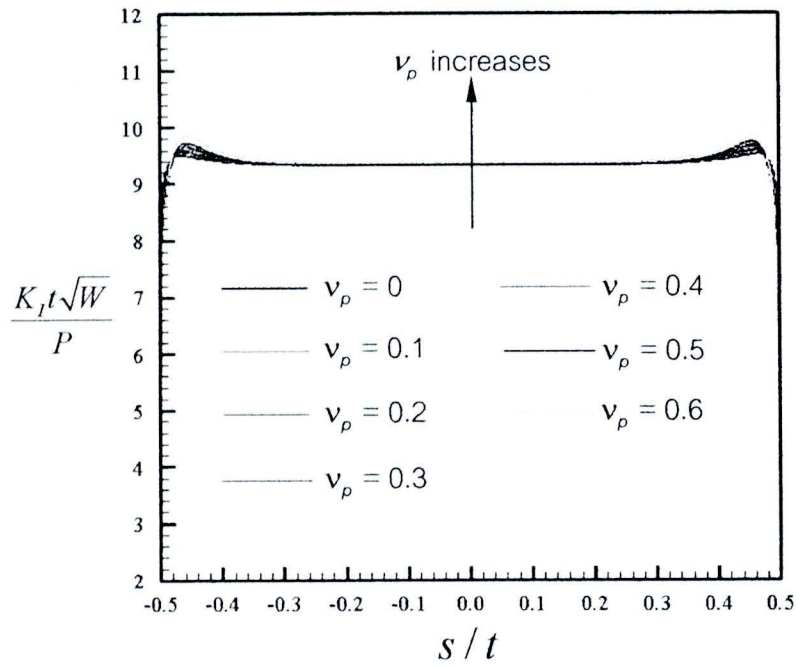

Figure 4.20 Normalized mode-I stress intensity factor versus the normalized distance along the crack front for various Poisson's ratios and $t/a = 40$

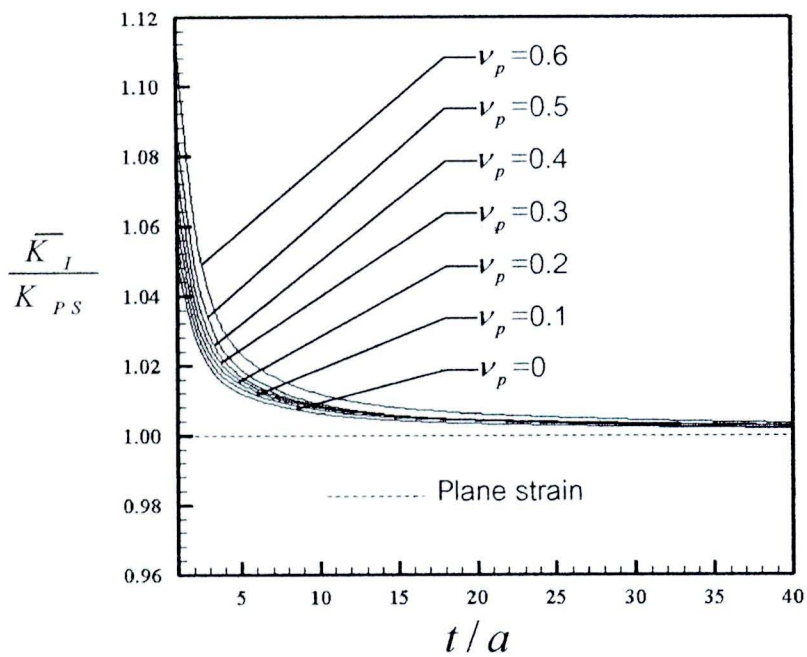

Figure 4.21 Normalized average stress intensity factor versus normalized thickness for different values of ν_p

4.2.3 Influence of modulus ratio E_p / E_z

Next, the influence of the modulus ratio E_p / E_z is investigated. In the analysis, five modulus ratios $E_p / E_z \in \{0.25, 0.5, 1, 2, 3\}$ are considered while other elastic constants remaining fixed. Again, those fixed material constants are taken from cadmium as shown in Table 4.1. Elastic constants associated with each modulus ratio employed in SGBEM are given in Table 4.3. It is important to emphasize that the value of ν_{pz} can readily be computed from the relation $\nu_{pz} = \nu_{zp}(E_p / E_z)$.

The normalized mode-I stress intensity factor is reported along the crack front for various thickness $t/a \in \{1, 2, 3, 5, 10, 20, 40\}$ in Figures 4.22-4.26 for $E_p / E_z \in \{0.25, 0.5, 1, 2, 3\}$, respectively. The plots between the normalized stress intensity and the normalized distance along the crack front for various modulus ratio $E_p / E_z \in \{0.25, 0.5, 1, 2, 3\}$ are also shown in Figures 4.27-4.30 for $t/a = 1, 5, 10, 40$, respectively. The modulus ratio E_p / E_z only slightly influences the distribution of the stress intensity factor along the crack front but significantly affects its magnitude. In addition, as the ratio E_p / E_z increases, the stress intensity factor tends to decreases.

The average stress intensity factor along the crack front is also reported for different values of E_p / E_z in Figure 4.31. It is obvious that the average stress intensity factor exhibits strong dependence on the modulus ratio and, in particular, as E_p / E_z increases, $\bar{K}_I$ increases and it requires larger specimen thickness in order to achieve the same value of $\bar{K}_I$.

Table 4.3 Elastic constants (GPa) associated with different values of modulus ratio E_p / E_z. The axis of material symmetry is taken to direct along x_3-coordinate direction.

Materials	E_{1111}	E_{1122}	E_{1133}	E_{3333}	E_{1313}
$E_p = 0.25E_z$	7.7	0.9	2.3	31.2	20.0
$E_p = 0.50E_z$	15.8	2.2	4.7	32.4	20.0
$E_p = E_z$	33.2	6.0	10.2	35.3	20.0
$E_p = 2E_z$	74.9	20.4	24.8	42.9	20.0
$E_p = 3E_z$	131.9	50.1	47.3	54.6	20.0

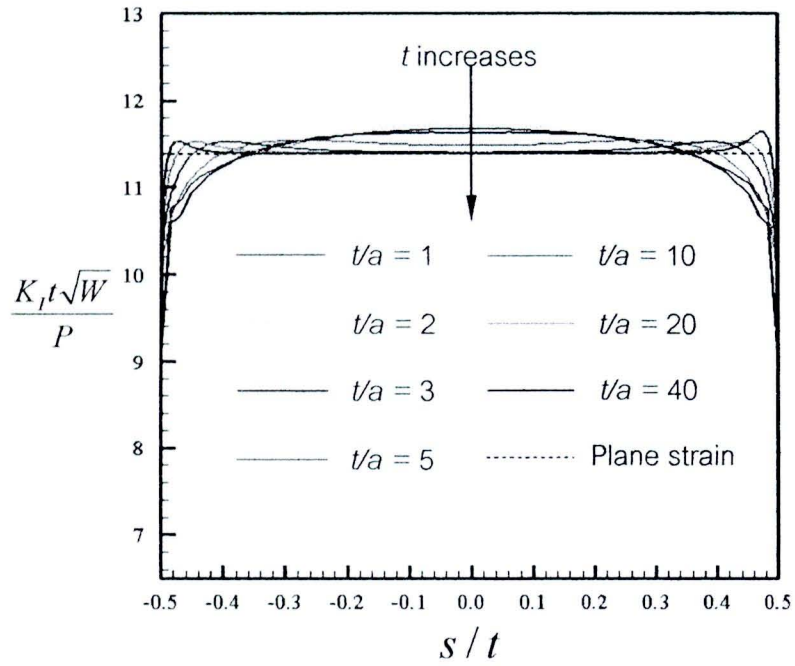

Figure 4.22 Normalized mode-I stress intensity factor versus the normalized distance along the crack front for various thicknesses and E_p / E_z = 0.25

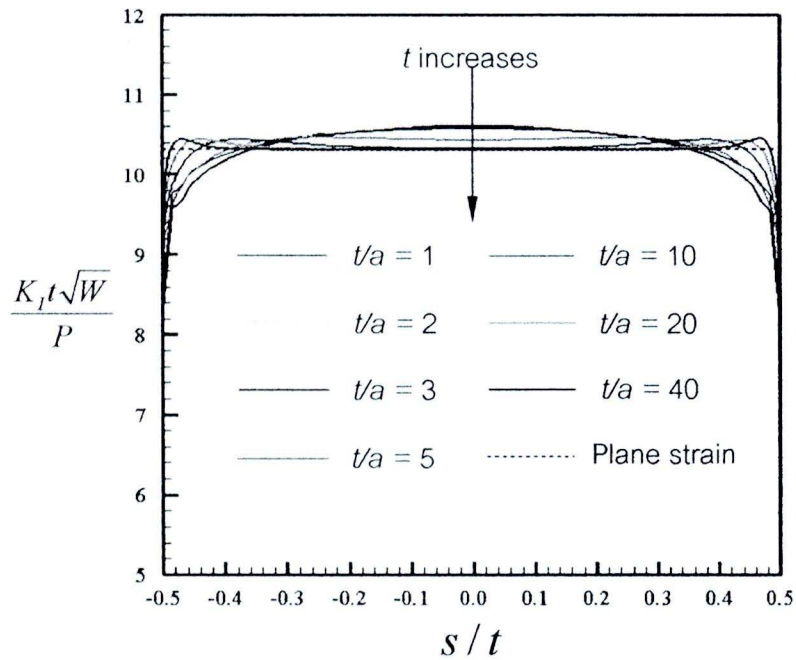

Figure 4.23 Normalized mode-I stress intensity factor versus the normalized distance along the crack front for various thicknesses and E_p / E_z = 0. 5

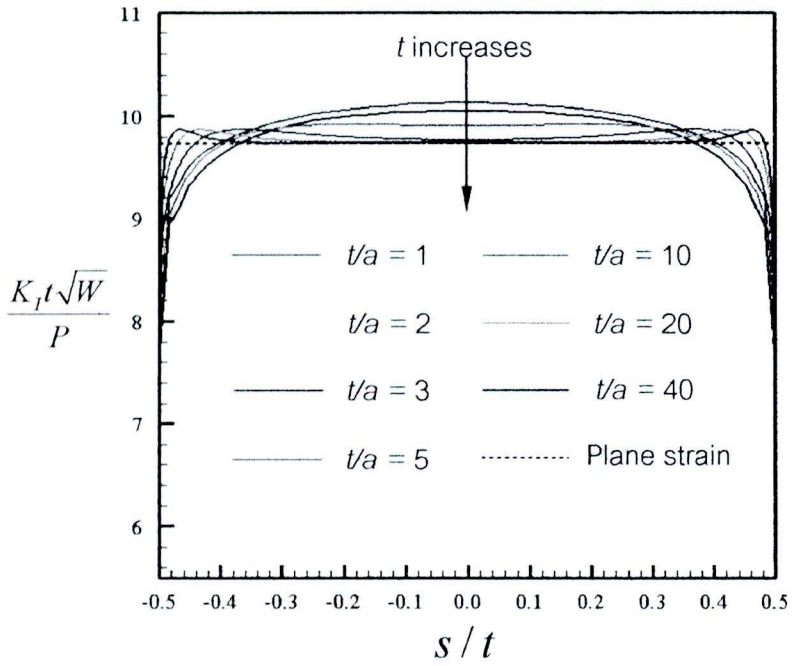

Figure 4.24 Normalized mode-I stress intensity factor versus the normalized distance along the crack front for various thicknesses and $E_p / E_z = 1$

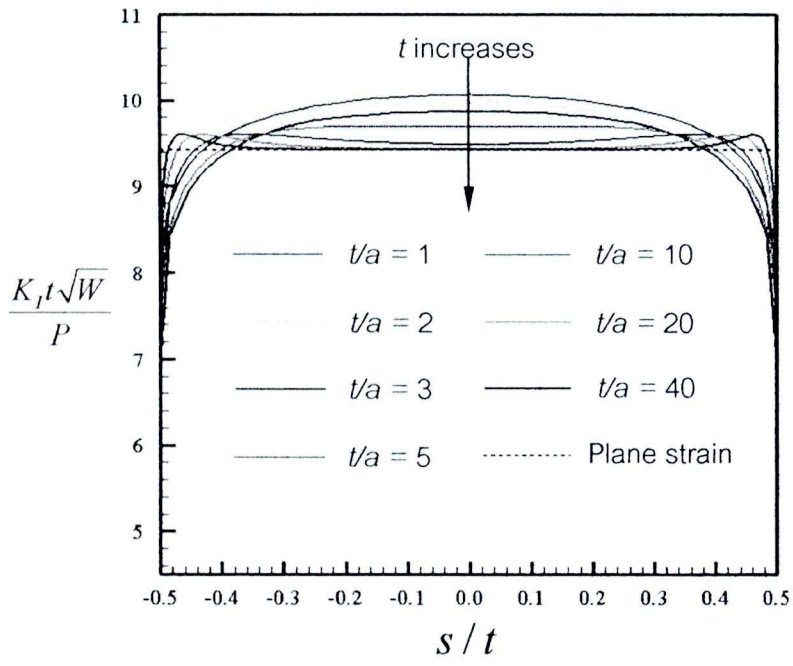

Figure 4.25 Normalized mode-I stress intensity factor versus the normalized distance along the crack front for various thicknesses and $E_p / E_z = 2$

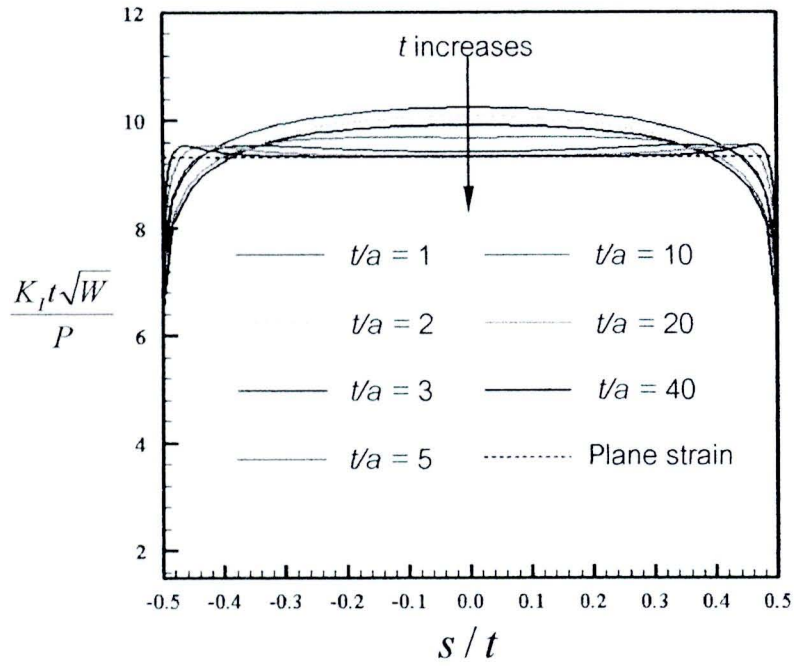

Figure 4.26 Normalized mode-I stress intensity factor versus the normalized distance along the crack front for various thicknesses and $E_p / E_z = 3$

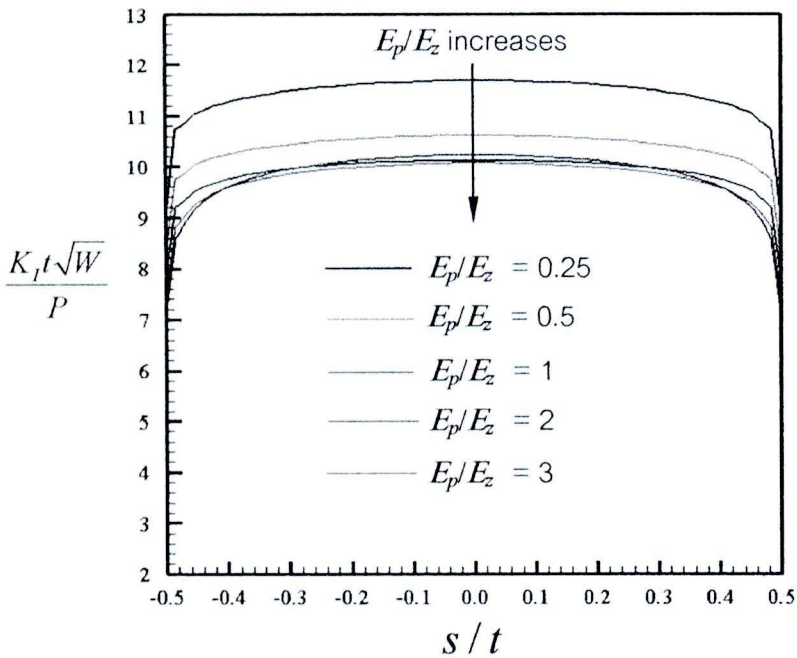

Figure 4.27 Normalized mode-I stress intensity factor versus the normalized distance along the crack front for various modulus ratios E_p / E_z and $t / a = 1$

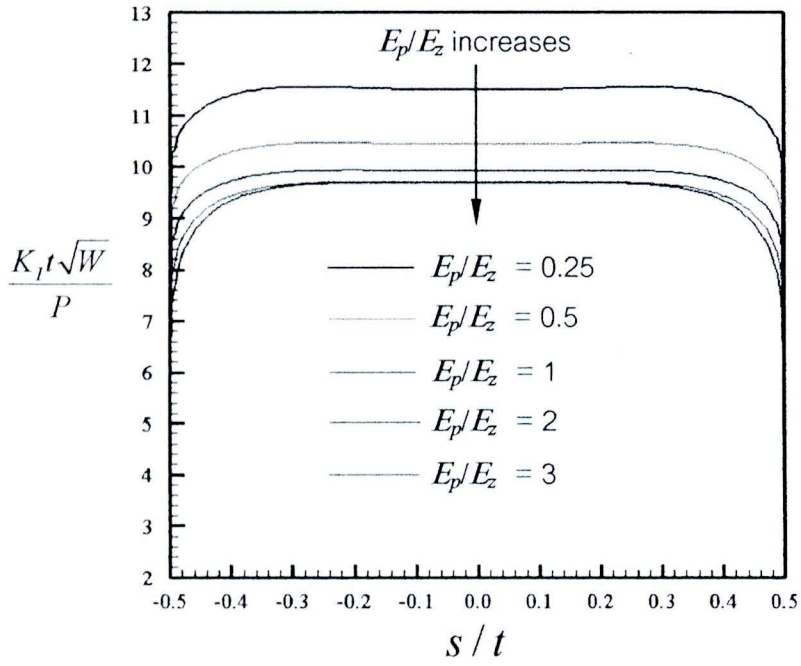

Figure 4.28 Normalized mode-I stress intensity factor versus the normalized distance along the crack front for various modulus ratios E_p / E_z and $t/a = 5$

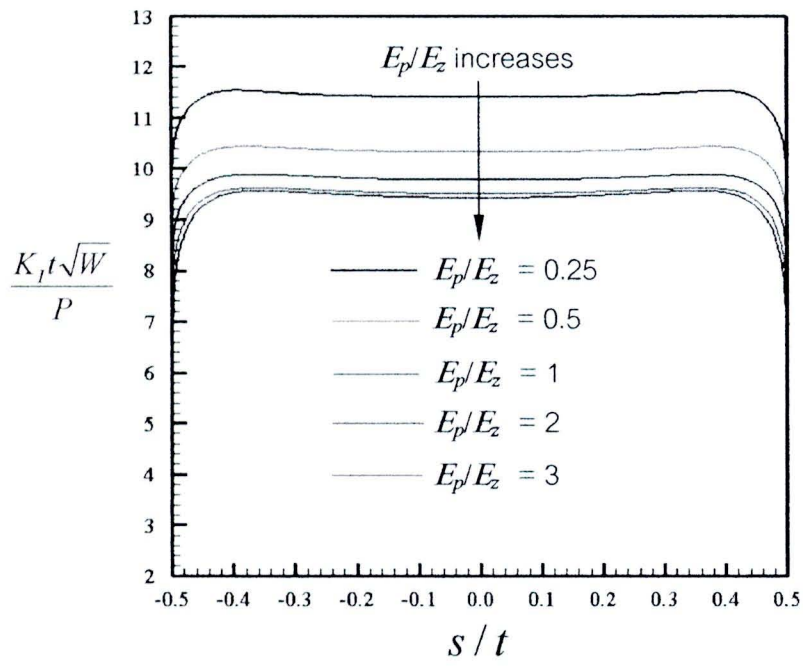

Figure 4.29 Normalized mode-I stress intensity factor versus the normalized distance along the crack front for various modulus ratios E_p / E_z and $t/a = 10$

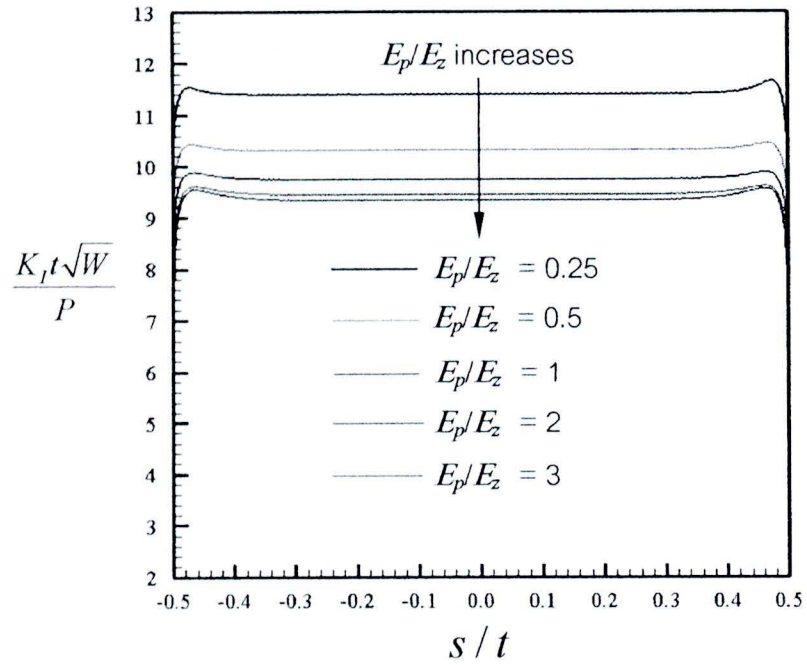

Figure 4.30 Normalized mode-I stress intensity factor versus the normalized distance along the crack front for various modulus ratios E_p / E_z and $t/a = 40$

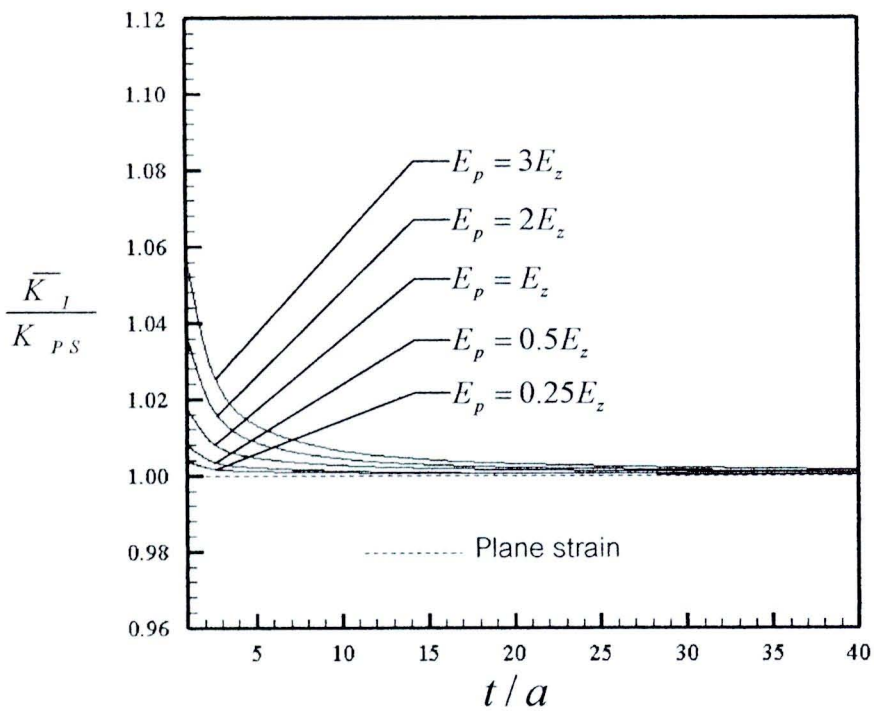

Figure 4.31 Normalized average stress intensity factor versus normalized thickness for different values of E_p / E_z

4.2.4 Influence of modulus ratio G_{zp}/E_p

Finally, we explore the influence of the modulus ratio G_{zp}/E_p. In the analysis, four values of the modulus ratio $G_{zp}/E_p \in \{0.25, 0.5, 1, 2\}$ are considered while other elastic constants remaining fixed. Again, those fixed material constants are taken from cadmium as given in Table 4.1. Elastic constants associated with each value of the modulus ratio employed in analysis by the SGBEM are given in Table 4.4. It is important to emphasize again that the value of ν_{pz} can readily be computed from the relation $\nu_{pz} = \nu_{zp}(E_p/E_z)$.

The normalized mode-I stress intensity factor is reported along the crack front for various thickness $t/a \in \{1, 2, 3, 5, 10, 20, 40\}$ in Figures 4.32-4.35 for $G_{zp}/E_p \in \{0.25, 0.5, 1, 2\}$, respectively. The plots between the normalized stress intensity and the normalized distance along the crack front for various modulus ratio $G_{zp}/E_p \in \{0.25, 0.5, 1, 2\}$ are also shown in Figures 4.36-4.39 for $t/a = 1, 5, 10, 40$, respectively. From these obtained results, similar behavior to the case of Poisson's ratio ν_p and modulus ratio E_p/E_z (e.g. the variation of the stress intensity near the vertex, the existence of the plane strain dominated zone in the central region of the crack front) is deduced when the thickness of the specimen increases. In addition, the modulus ratio G_{zp}/E_p only slightly influences the distribution of the stress intensity factor along the crack front but strongly affects its magnitude. The stress intensity factor tends to increases as the modulus ratio G_{zp}/E_p increases.

The average stress intensity factor along the crack front is also reported for different values of G_{zp}/E_p in Figure 4.40. It is obvious from this set of results that the average stress intensity factor exhibits only slightly dependence on the modulus ratio G_{zp}/E_p and it decays monotonically to the plane strain value as the specimen thickness increases.

Table 4.4 Elastic constants (GPa) associated with different values of modulus ratio G_{zp}/E_p. The axis of material symmetry is taken to direct along the x_3-coordinate direction.

Materials	E_{1111}	E_{1122}	E_{1133}	E_{3333}	E_{1313}
$G_{zp}=0.25E_p$	116.6	41.2	41.0	51.3	20.8
$G_{zp}=0.50E_p$	116.6	41.2	41.0	51.3	41.5
$G_{zp}=E_p$	116.6	41.2	41.0	51.3	83.0
$G_{zp}=2E_p$	116.6	41.2	41.0	51.3	166.0

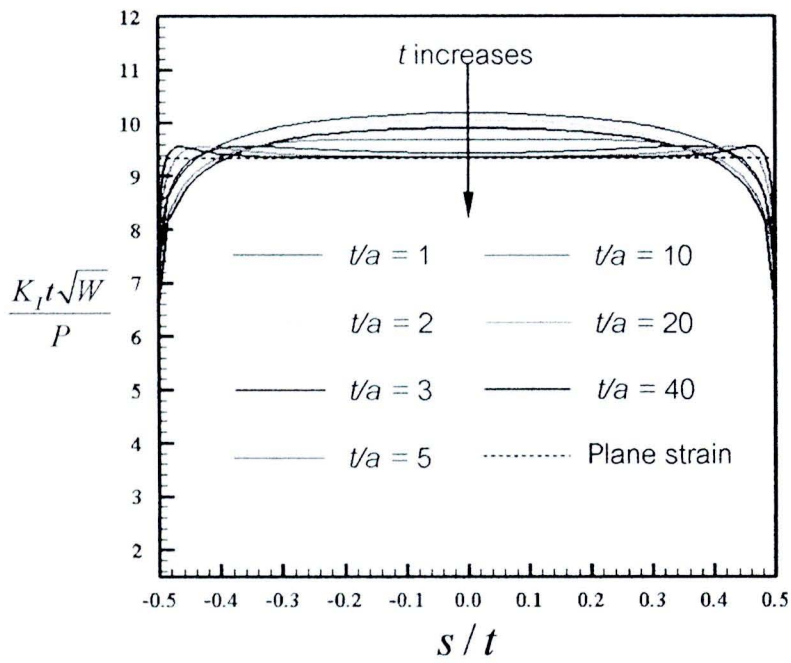

Figure 4.32 Normalized mode-I stress intensity factor versus the normalized distance along the crack front for various thicknesses and G_{zp}/E_p = 0.25

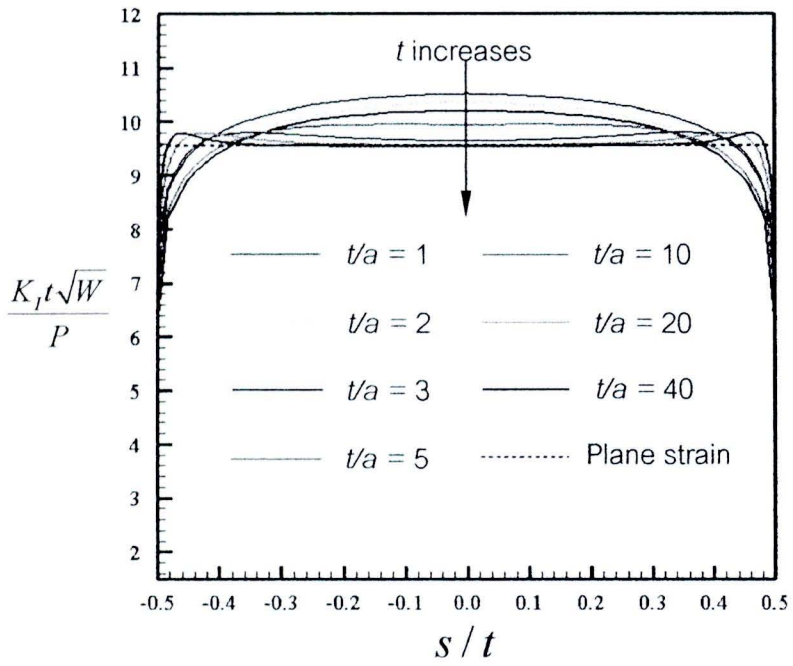

Figure 4.33 Normalized mode-I stress intensity factor versus the normalized distance along the crack front for various thicknesses and $G_{zp} / E_p = 0.5$

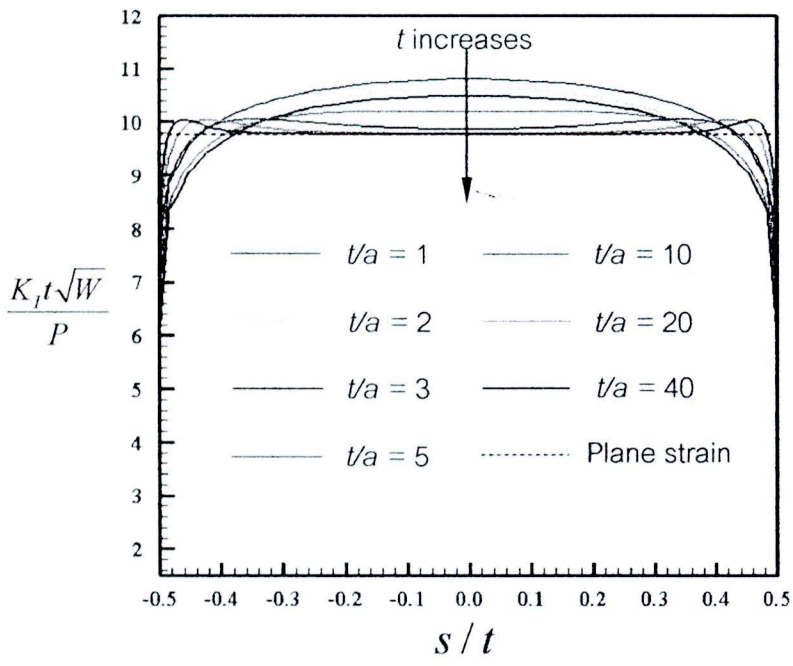

Figure 4.34 Normalized mode-I stress intensity factor versus the normalized distance along the crack front for various thicknesses and $G_{zp} / E_p = 1$

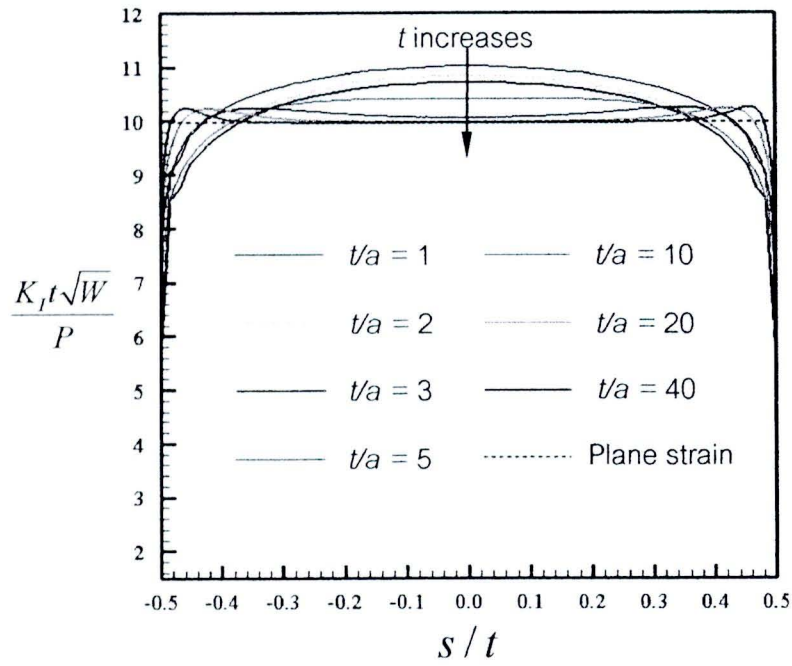

Figure 4.35 Normalized mode-I stress intensity factor versus the normalized distance along the crack front for various thicknesses and $G_{zp} / E_p = 2$

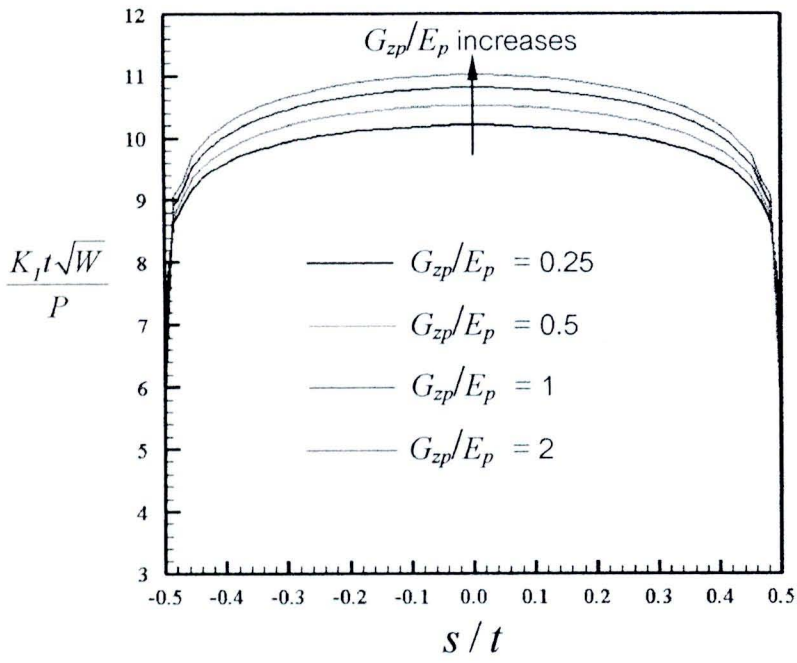

Figure 4.36 Normalized mode-I stress intensity factor versus the normalized distance along the crack front for various modulus ratios G_{zp} / E_p and $t / a = 1$

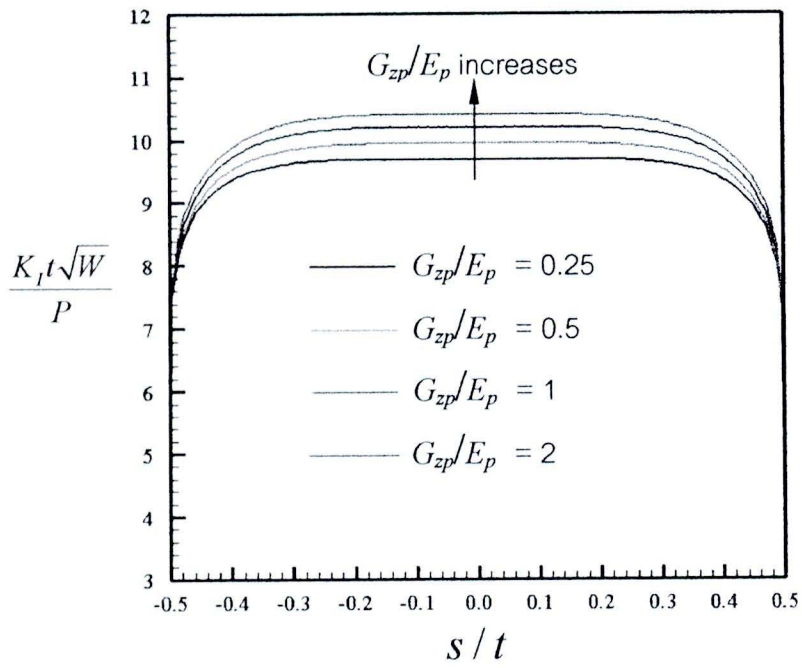

Figure 4.37 Normalized mode-I stress intensity factor versus the normalized distance along the crack front for various modulus ratios G_{zp}/E_p and $t/a = 5$

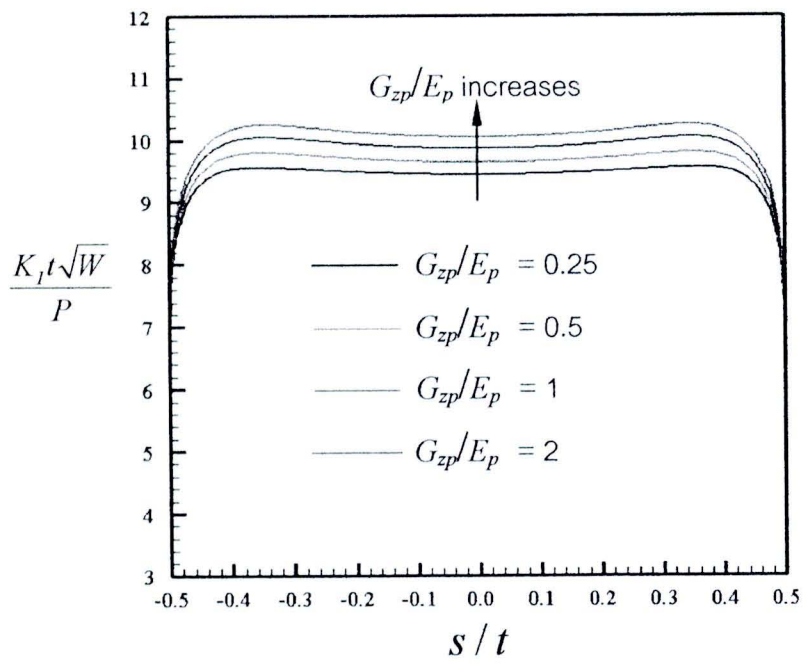

Figure 4.38 Normalized mode-I stress intensity factor versus the normalized distance along the crack front for various modulus ratios G_{zp}/E_p and $t/a = 10$

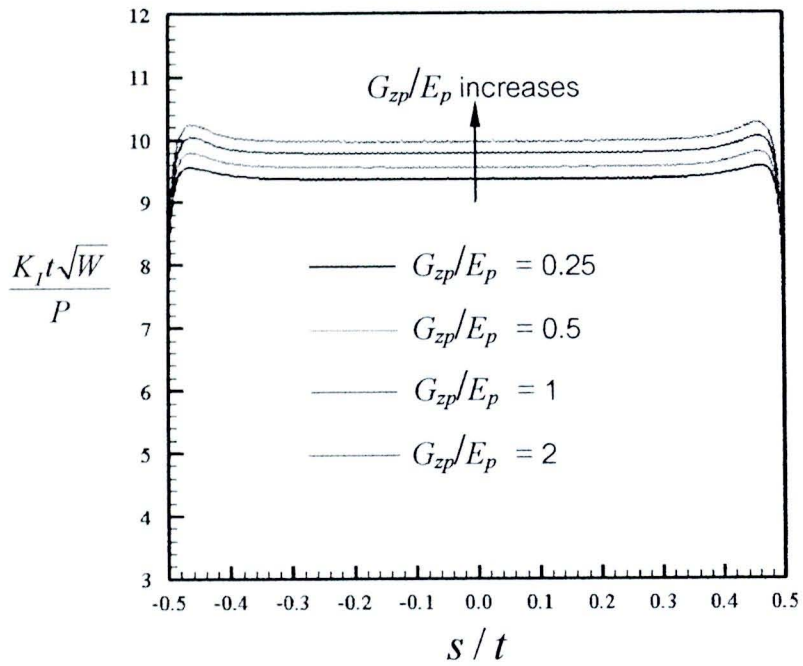

Figure 4.39 Normalized mode-I stress intensity factor versus the normalized distance along the crack front for various modulus ratios G_{zp}/E_p and $t/a = 40$

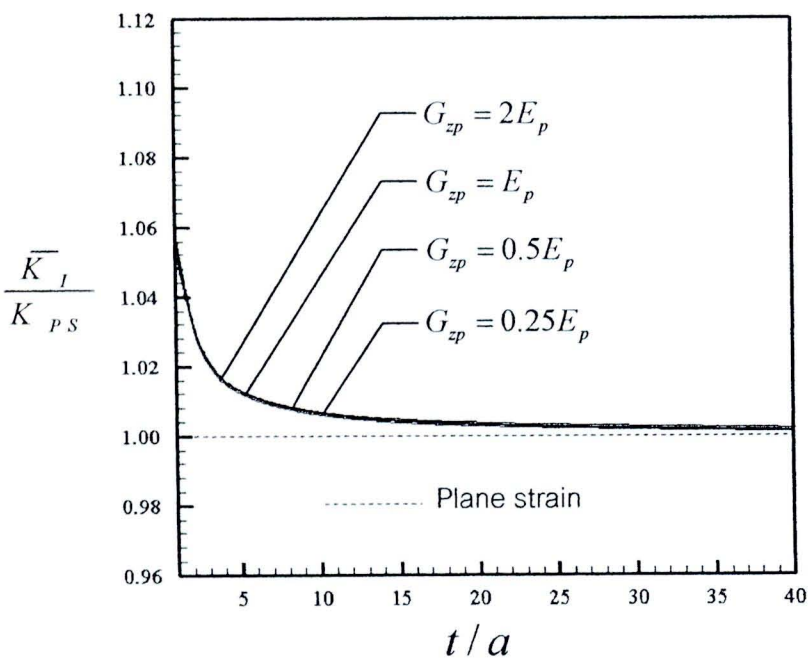

Figure 4.40 Normalized average stress intensity factor versus normalized thickness for different values of G_{zp}/E_p